Elsevier Editorial System(tm) for Journal of Electroanalytical Chemistry

Manuscript Draft

Manuscript Number: JELECHEM-D-20-00560R1

Title: Blue LED light-driven photoelectrocatalytic removal of naproxen from water: Kinetics and primary by-products

Article Type: Short Communication

Keywords: Blue LED light; Oxidation by-products; Pharmaceutical residue; Photoelectrocatalysis; Water treatment

Corresponding Author: Dr. Ignasi Sires, Ph.D.

Corresponding Author's Institution: Universitat de Barcelona

First Author: Katherina Changanaqui, MsC.

Order of Authors: Katherina Changanaqui, MsC.; Hugo Alarcón, Ph.D.; Enric Brillas, Ph.D.; Ignasi Sires, Ph.D.

Abstract: Here, we demonstrate the viability of a ZnO/TiO2/Ag2Se thin-film composite synthesized on FTO to degrade the drug naproxen in aqueous solutions by visible-light photoelectrocatalysis (PEC). The experiments were made with 100 mL of solutions containing 5 mg L-1 drug and 50 mM Na2SO4 at natural pH, using a cell equipped with a Pt wire as cathode and the composite as photoanode exposed to a 36 W blue LED lamp. Total degradation was achieved after 210 min of electrolysis at anodic potential of +1.0 V/Ag|AgCl. This resulted from the oxidative action of hydroxyl radicals formed via direct anodic water discharge and through mediated water oxidation by photogenerated holes. The degradation rate decreased at higher naproxen concentration, but the treatment efficiency became higher due the deceleration of the parasitic reactions involving hydroxyl radicals. In chloride medium, the photoanode showed a large ability to produce active chlorine, which contributed to the oxidation of the target molecule. LC-QToF-MS analysis of treated solutions revealed the generation of four primary naphthalenic by-products, from which the initial degradation route of naproxen is proposed.

Blue LED light-driven photoelectrocatalytic removal of naproxen from water: Kinetics and primary by-products

Katherina Changanaqui [a,b], Hugo Alarcón [b], Enric Brillas [a], Ignasi Sirés [a,*]

[a] *Laboratori d'Electroquímica dels Materials i del Medi Ambient, Departament de Química Física, Facultat de Química, Universitat de Barcelona, Martí i Franquès 1-11, 08028 Barcelona, Spain*

[b] *Centro de Desarrollo de Materiales Avanzados y Nanotecnología, Universidad Nacional de Ingeniería, Av. Túpac Amaru 210, Rímac, Lima, Peru*

*Corresponding author: E-mail address: i.sires@ub.edu (I. Sirés)

Abstract

Here, we demonstrate the viability of a $ZnO/TiO_2/Ag_2Se$ thin-film composite synthesized on FTO to degrade the drug naproxen in aqueous solutions by visible-light photoelectrocatalysis (PEC). The experiments were made with 100 mL of solutions containing 5 mg L^{-1} drug and 50 mM Na_2SO_4 at natural pH, using a cell equipped with a Pt wire as cathode and the composite as photoanode exposed to a 36 W blue LED lamp. Total degradation was achieved after 210 min of electrolysis at anodic potential of +1.0 V/Ag|AgCl. This resulted from the oxidative action of hydroxyl radicals formed via direct anodic water discharge and through mediated water oxidation by photogenerated holes. The degradation rate decreased at higher naproxen concentration, but the treatment efficiency became higher due the deceleration of the parasitic reactions involving hydroxyl radicals. In chloride medium, the photoanode showed a large ability to produce active chlorine, which contributed to the oxidation of the target molecule. LC-QToF-MS analysis of treated solutions revealed the generation of four primary naphthalenic by-products, from which the initial degradation route of naproxen is proposed.

Keywords Blue LED light; Oxidation by-products; Pharmaceutical residue; Photoelectrocatalysis; Water treatment

1. Introduction

The development of more effective technologies for the removal of pharmaceutical residues as well as their metabolites and natural degradation products from water has been intensified in the last decade [1-3]. A large variety of pharmaceuticals is continuously discharged to the aquatic ecosystems as a result of their massive use in human and veterinary medicine [4]. The presence of such pollutants, usually at μg L^{-1} level, severely affects the quality of drinking water and the health of all living beings [5,6]. It has been confirmed that they cannot be completely removed in conventional water treatment facilities [2,7] and hence, more powerful technologies are required.

Non-steroid anti-inflammatory drugs (NSAIDs) are commonly consumed to release pain and fever, being naproxen (NPX, (+)-(*S*)-2-(6-methoxynaphthalen-2-yl)propanoic acid) one of the most prescribed among them. The presence of NPX and its metabolites in natural water and urban wastewater has been documented, alongside its toxic effects on different organisms [8]. Several advanced oxidation processes (AOPs), which involve the reaction with a strong oxidant like hydroxyl radical ($^{\bullet}$OH) generated on site, have been proven to be highly effective for NPX degradation. Some examples include: (i) electrochemical oxidation (EO) with anodes like boron-doped diamond (BDD) [9,10], Pt nanoparticles (NPs) [11] or multi-walled carbon nanotubes [12], (ii) electrochemical Fenton-based processes like electro-Fenton [10,13] and photoelectro-Fenton [10], (iii) photocatalysis (PC) with TiO_2 [13,14], S/W co-doped $BiVO_4$ [15] and N-doped TiO_2 [16], and (iv) photoelectrocatalysis (PEC) with a Bi_2/MoO_6-BDD photoanode [17].

EO is the simplest electrochemical AOP, being its oxidation power mainly modulated by the anode (M) nature. Physisorbed hydroxyl radical is formed from water discharge via reaction (1) [18]. Non-active anodes like BDD outperform the others due to their larger overpotential for O_2 evolution. In some media like those rich in chloride, other strong

oxidants can be simultaneously formed. Active chlorine (HClO in the pH range 3.0-8.0) is produced from anodic oxidation of Cl^- via reaction (2) followed by hydrolysis reaction (3) [19]. Under such conditions, the organics are competitively degraded by both, M($^\bullet$OH) and active chlorine.

$$M + H_2O \rightarrow M(^\bullet OH) + H^+ + e^- \quad (1)$$

$$2Cl^- \rightarrow Cl_2 + 2e^- \quad (2)$$

$$Cl_2 + H_2O \rightarrow HClO + Cl^- + H^+ \quad (3)$$

EO is particularly useful to treat wastewater with relatively high organic load. Conversely, PC is more appropriate to remove organic pollutants at small concentration [20]. This technique is based on the exposure of a semiconductor to photons having an energy superior to that of its bandgap (E_{gap}), which promotes an electron from the valence to the conduction band. Reaction (4) represents the production of charge carriers on the photocatalyst surface, i.e., a hole at the valence band (h_{VB}^+) and an electron at the conduction band (e_{CB}^-) [16,21]. In inert media, the oxidation of the organic molecules occurs preferentially by the attack of P($^\bullet$OH), formed from h_{VB}^+-mediated water oxidation via reaction (5). However, the oxidation power of PC is limited by the fast recombination of the e_{CB}^-/h_{VB}^+ pair. This drawback can be overcome by means of PEC process, in which the photocatalyst acts as the anode of an electrochemical cell. It still allows the occurrence of reaction (1) but, in addition, the photogenerated e_{CB}^- is drained to the cathode, thus minimizing the destruction of h_{VB}^+ and eventually enhancing the P($^\bullet$OH) production [20,22].

$$\text{Photocatalyst} + h\nu \rightarrow h_{VB}^+ + e_{CB}^- \quad (4)$$

$$\text{Photocatalyst} + h_{VB}^+ + H_2O \rightarrow P(^\bullet OH) + H^+ \quad (5)$$

The most commonly used photocatalyst is TiO_2 in its anatase form, with an E_{gap} = 3.2 eV (λ = 387 nm) [20]. This material requires UV light, which represents < 5% of solar spectrum, for optimum photoexcitation. Several attempts have been made to extend the photon absorption to the visible range (λ > 400 nm), such as decoration with noble metals like Ag [22] and Au [23,24]. Recently, we have developed a new photocatalyst composed of ZnO nanorods (NRs) coated with TiO_2 and further decorated with electrodeposited Ag_2Se NPs [25]. The NRs provide a large surface area, TiO_2 confer a larger photostability and the Ag_2Se NPs (E_{gap} = 1.85 eV) allow the absorption of visible photons. The ability of PEC with the $ZnO/TiO_2/Ag_2Se$ composite on fluoride-doped tin oxide (FTO) to destroy the antibiotic oxytetracycline in urban wastewater was demonstrated, but more research is needed to confirm the viability of the system for drug removal.

This work presents a study on the degradation of NPX solutions at natural pH by means of visible-light PEC. First, the presence of the Ag_2Se NPs was corroborated by high-resolution transmission electron microscopy (HRTEM). Comparative EO and PC trials in sulfate medium were carried out to clarify the role of the different oxidizing agents in PEC process. In this medium, the effect of NPX concentration on PEC performance was examined. The influence of active chlorine in Cl^- medium was considered as well. Finally, an initial degradation route for NPX in sulfate medium has been proposed considering the by-products detected by liquid chromatography quadrupole time-of-flight mass spectrometry (LC-QToF-MS).

2. Materials and methods

Naproxen sodium ($NaC_{14}H_{13}O_3$, M = 252.24 g mol^{-1}, ~ 100% purity) was acquired from Sigma-Aldrich. TEC7 FTO glass wafers were from Dyesol Australia. Analytical grade Na_2SO_4 and NaCl were purchased from Fluka. Solutions were prepared with Millipore Milli-

Q ultrapure water. All the syntheses and analyses were made with HPLC or analytical grade chemicals purchased from Alfa Aesar, Panreac, Sigma-Aldrich and Merck.

The FTO/ZnO/TiO_2/Ag_2Se thin-film photoanode was prepared following the procedure reported in earlier work [25]. Briefly, the FTO substrate with dimensions of 2.5 cm × 2.0 cm was first pre-treated and then placed as the cathode of an electrolytic cell to deposit $Zn(OH)_2$ seeds from a 0.10 mM $Zn(CH_3COO)_2$ solution at 70 ºC by applying a cathodic potential (E_{cath}) = -1.1 V/Ag|AgCl for 180 s. After calcination at 400 ºC for 2 h, the ZnO NRs were grown upon immersion in a 0.15 mM $Zn(NO_3)_2$ + 0.80 M NaOH supernatant solution at 90 ºC for 75 min. The resulting ZnO thin film onto FTO was immersed in an alkaline colloidal TiO_2 suspension, prepared with Ti(IV) isopropoxide at pH 11, at 5 cm min^{-1} and after 10 min it was retrieved at the same rate. The sample was dried at 100 ºC for 10 min and calcined at 550 ºC for 1 h. The whole procedure was repeated to obtain 3 layers. Finally, Ag_2Se NPs were electrodeposited onto the FTO/ZnO/TiO_2 composite via immersion in $AgNO_3$ + H_2SeO_3 solution at pH 3.0 and 25 ºC, applying an E_{cath} = -0.65 V/Ag|AgCl for 600 s.

To confirm the integrity and morphological properties of the resulting thin films, the samples were characterized by HRTEM employing a JEOL JEM-2100 LaB6 microscope with energy-dispersive X-ray spectroscopy (EDX), operating at 200 kV in scanning TEM (i.e., STEM) mode. For these analyses, the films were scratched out from the substrate. Additionally, the sample was prepared for cross-sectional analysis: it was cut into two pieces, which were glued together (active side on), then the ensemble was mechanically polished in the perpendicular direction and finally thinned via ion milling upon attack by two Ar^+ guns at 7º and 5 kV. HRTEM images and electron energy loss spectroscopy (EELS) spectra were acquired in high-angle annular dark-field (HAADF) STEM mode, clearly revealing the elemental distribution in the NRs.

An undivided three-electrode cell, equipped with a jacket to keep the solution temperature at 25 ºC by recirculating thermostated water, was used to treat 100-mL solutions by EO, PC and PEC under magnetic stirring at 600 rpm. The anode or photoanode was the synthesized FTO/ZnO/TiO_2/Ag_2Se thin film, the cathode was a Pt wire and the reference electrode was an Ag|AgCl (saturated KCl). PC assays were carried out in the absence of current flow, whereas in EO and PEC an anodic potential (E_{anod}) = +1.0 V/Ag|AgCl was provided by an Amel 2049 potentiostat-galvanostat. In PC and PEC trials, the photocatalyst thin film was exposed to irradiation from a Highgrow 36 W blue LED lamp, composed of LED light bulbs of 2 W arranged in a grid, placed at 7 cm. The irradiance from the lamp was 173 W m^{-2} at λ_{max} = 450-460 nm. Between two consecutive runs, the FTO/ZnO/TiO_2/Ag_2Se was rinsed with Milli-Q water, which ensured the obtention of reproducible duplicates for drug concentration decays. Average values are given in this work, with error bars depicted in each curve. In photo-assisted trials, the entire system was embedded inside a mirror box to upgrade the photon collection.

The pH measurement, reversed-phase high-performance liquid chromatography (HPLC) analysis to monitor the NPX concentration, and LC-QToF-MS analysis to detect the primary by-products of NPX in PEC trials, were made with the same equipment and procedures reported elsewhere [25]. In reversed-phase HPLC, a BDS Hypersil C18 5μm (250 mm × 4.6 mm) column at 35 ºC, and a mobile phase composed of 40:60 (v/v) CH_3CN/H_2O (0.010 M KH_2PO_4) at pH 3.0 and eluted at 1.0 mL min^{-1}, were employed, yielding a sharp peak for NPX (λ = 231 nm) at a retention time of 5.0 min, with a limit of quantification of 5 μg L^{-1}.

3. Results and discussion

3.1. Comparative degradation of NPX in sulfate medium by EO, PC and PEC

147 The physicochemical, photochemical, morphological and structural characteristics of the
148 as-synthesized FTO/ZnO/TiO_2/Ag_2Se thin-film composite have been described in our earlier
149 work [25]. Aiming to further complete those characterizations, a more detailed HRTEM
150 analysis has been carried out, as shown in Fig. 1. In one of the sample replicates prepared, the
151 coating was scratched out and its morphology can be observed in Fig. 1a. NRs with a length
152 of several hundreds of microns are clearly identified, being their walls decorated with quite
153 rounded NPs as that highlighted in yellow. The second replicate served to do a cross-sectional
154 analysis. A certain alignment of the NRs on the FTO can be seen in Fig. 1b, where one of the
155 NPs is highlighted in blue. A closer view in Fig. 1c allows identifying a certain degree of NRs
156 entanglement, probably due to the sample preparation, and a total length greater than 500 nm,
157 which agrees with that found in our previous work. In this HAADF-STEM cross-sectional
158 micrograph of the photoanode, several spots are distributed along the NRs. The EELS
159 analysis of one of them, highlighted as a brighter spot, informs about the elemental
160 distribution. It corroborates that the rounded NPs that decorate the rods are rich in Ag and Se
161 (see the maximum intensity of both elements in the bright spot area), whereas the rods are
162 rich in Ti and O as corresponds to the presence of the TiO_2 layers coating the underlying ZnO.
163 First degradation tests were made with 100 mL of solutions containing 5.0 mg L^{-1} NPX
164 and 50 mM Na_2SO_4 at natural pH 5.7 and 25 ºC. According to Fig. 2a, the drug underwent a
165 continuous but very slow abatement by EO at E_{anod} = +1.0 V/Ag|AgCl for 210 min, ending in
166 a degradation as low as 12.0%. An analogous trial was made in parallel, at E_{anod} = 0 V,
167 causing no drug removal, which allowed discarding a relevant adsorption on the thin-film
168 photoanode. Therefore, the trend observed in EO can be explained by the active nature of the
169 anode, which implies a very low production of oxidant M($^{\bullet}$OH) from reaction (1) [3,10]. A
170 much quicker and greater NPX removal, finally reaching 51.3% decay, can be observed for
171 the PC process. This means that a comparatively larger amount of oxidant P($^{\bullet}$OH) was

generated from reaction (5), significantly contributing to the removal. Fig. 2a highlights that both methods cannot compete with PEC process, which allowed the total disappearance of the drug in 210 min. This suggests the occurrence of a synergistic phenomenon, yielding an abatement much superior to that arising from the sum of single EO and PC. This behavior agrees with the expected acceleration of P($^{\bullet}$OH) production as result of the substantial inhibition of the e_{CB}^{-}/h_{VB}^{+} recombination [20,22,26].

The fitting of the above concentration decays was attempted by means of kinetic equations with different reaction orders, obtaining the best linear profiles for a pseudo-first-order reaction, as can be seen in Fig. 2b. This kind of behavior can be interpreted assuming that a steady content of M($^{\bullet}$OH) and/or P($^{\bullet}$OH) is responsible for the drug destruction during each treatment. It should be noted that the solution pH remained practically constant in each run, and reproducible profiles (see errors in Fig. 2a) were obtained by simply rinsing the thin film with Milli-Q water before further use. From the analysis of Fig. 2b, the pseudo-first-order rate constant (k_1) for NPX decay and the corresponding R^2-value were determined. All these results are summarized in Table 1. As can be seen, excellent regressions ($R^2 > 0.98$) were always obtained, and the k_1-value of 0.0126 min^{-1} in PEC was 3.5-fold and 21.5-fold greater than those found in PC and EO, confirming the synergy between light irradiation and current supply for drug removal.

3.2. Effect of NPX concentration on PEC performance in sulfate medium

The influence of NPX content on the PEC degradation power in sulfate medium was investigated by employing solutions with 50 mM Na_2SO_4 and drug concentrations ranging from 2.0 to 5.0 mg L^{-1} at natural pH. They were treated by PEC at E_{anod} = +1.0 V/Ag|AgCl, for 210 min as maximal. No substantial pH variation was observed in these runs, which showed a high reproducibility just following a simple cleaning procedure before each subsequent electrolysis.

Fig. 3 shows the profiles of the normalized concentration removals during such assays, alongside the corresponding excellent pseudo-first-order kinetic analyses in the inset panel. A gradually lower degradation rate can be observed as the drug content was increased, with overall disappearance at about 180 min when starting at 2.0 mg L^{-1} and a progressive increase in time up to 210 min needed at 5.0 mg L^{-1} (see Table 1). As expected, the k_1-value also collected in Table 1 decreased from 0.0273 to 0.0126 min^{-1} when the NPX concentration grew from 2.0 to 5.0 mg L^{-1}, pointing to consider that k_1 was a function of the number of oxidizing agents available in practice for NPX oxidation in each treatment. Worth noting, the oxidation power of the system in practice was raised at higher NPX concentration, as deduced from the fact that a gradually larger quantity of drug was removed. For example, after 180 min of PEC treatment, 2.0, 3.0, 3.95 and 4.74 mg L^{-1} of NPX were destroyed starting at 2.0, 3.0, 4.0 and 5.0 mg L^{-1}, respectively. This enhancement is not surprising, since it is typically found in EAOPs [3]. It can be accounted for by the deceleration of parasitic reactions that cause the destruction of generated M($^{\bullet}$OH) and P($^{\bullet}$OH); consequently, a greater number of fruitful reactive events occurs, thus removing a larger number of organic molecules. Among those parasitic reactions that waste the $^{\bullet}$OH one can include, for example, its anodic oxidation to O_2 or its dimerization to H_2O_2 [10,19]. The above results demonstrate the ability of the FTO/ZnO/TiO_2/Ag_2Se photoanode to degrade NPX. This performance is better than that reported by Zhao et al. [17], who achieved 85% degradation after 360 min of treatment of 60 mL of 15 mg L^{-1} drug solutions with 0.1 M Na_2SO_4 using a porous Bi_2/MoO_6-BDD photoanode (E_{anod} = +2.0 V/SCE) exposed to a 150 W Xe lamp (filtered at $\lambda > 420$ nm).

3.3. Influence of Cl^- concentration on PEC treatment

The influence of Cl^- ion presence in the aqueous matrix on the degradation process was assessed with 5.0 mg L^{-1} NPX treated by PEC at E_{anod} = +1.0 V/Ag|AgCl for 210 min. Two solutions containing chloride, namely 25 mM Na_2SO_4 + 35 mM NaCl and 70 mM NaCl, were

chosen since they possessed the same specific conductivity as the 50 mM Na_2SO_4 solution [19]. Again, no substantial pH changes were observed and the degradation profiles were quite reproducible at least in two consecutive trial replicates.

A surprising tendency is evidenced in Fig. 4, since the degradation rate in the mixed sulfate + chloride matrix was lower than that attained in pure sulfate, whereas the assays in pure chloride became significantly better than the others (see also Table 1). This suggests a fast attack of P($^{\bullet}$OH) formed from reaction (5), and even faster by HClO formed from reaction (3), at high Cl^- content (70 mM), becoming more rapid than that of M($^{\bullet}$OH) and P($^{\bullet}$OH) that are prevalent in sulfate medium. In contrast, a smaller amount of hydroxyl radicals and HClO was available in the mixed sulfate + chloride matrix, because of their mutual destruction that ended in the generation of much less powerful chlorine and oxychlorine radicals that react more slowly with the drug.

The inset of Fig. 4 illustrates the pseudo-first-order reaction also followed in the media with presence of chloride. This is indicative of the attack of constant and small quantities of M($^{\bullet}$OH), P($^{\bullet}$OH) and/or HClO over NPX. The k_1-values given in Table 1 disclose a 1.3-fold enhancement in 70 mM NaCl as compared to 50 mM Na_2SO_4. This corroborates the electrocatalytic ability of the FTO/ZnO/TiO_2/Ag_2Se thin-film photoanode to oxidize Cl^- via the anodic reaction (2), allowing the production of sufficient amounts of HClO that rapidly attack the drug. As a first assessment of the durability of the photoanode, five consecutive runs of 210-240 min were carried out in pure chloride medium, finding quite reproducible profiles.

It should be noted that the change of total organic carbon content with time in all the above assays was not evaluated due to its very low initial value (i.e., 3.6 mg C L^{-1} at 5.0 mg L^{-1} NPX). Nevertheless, a quicker mineralization should occur in sulfate medium, because in chloride media the formation of recalcitrant chloro-derivatives is expected [26].

247 *3.4. Detection and evolution of by-products and proposed initial degradation route*

248 LC-QToF-MS analysis of a 5.0 mg L^{-1} NPX (**1**, *m/z* 230) solution with 50 mM Na_2SO_4 at
249 natural pH 5.7 treated by PEC under the conditions of Fig. 2a revealed the formation of four
250 derivatives with *m/z* values of 246, 185, 201 and 202. These values matched with those
251 expected for naphthalenic molecules like the hydroxylated NPX (compound **2**), 2-methoxy-6-
252 vinylnaphthalene (compound **3**), its hydroxylated derivative (compound **4**) and 6-methoxy-2-
253 naphthoic acid (compound **5**), respectively. Note that compounds **3** and **5** have been detected
254 as oxidation by-products of NPX during electro-Fenton and photoelectro-Fenton treatments
255 [10].

256 Fig. 5 shows the evolution of these compounds while the target molecule disappeared
257 from the medium. As can be seen, compound **2** was rapidly generated, thereby being
258 completely removed at 240 min. In contrast, the other three compounds were gradually
259 accumulated, thus accounting for a larger stability and slower destruction rate. That means
260 that a long time will be needed to achieve a large mineralization.

261 Based on the detected by-products, a plausible route for the initial NPX degradation by
262 PEC in sulfate medium is schematized in Fig. 6. The oxidizing agents are the generated
263 M($^{\bullet}$OH) and P($^{\bullet}$OH), which are simply denoted as $^{\bullet}$OH in the scheme. The process is initiated
264 either by the hydroxylation of **1** to yield **2** or its decarboxylation to form **3**. Further
265 hydroxylation of **3** leads to **4**, whereas the oxidation of its vinyl group yields **5**. After this
266 stage, the cleavage of the naphthalene ring of these compounds would generate final short-
267 chain linear carboxylic acids that are mineralized to CO_2, as has been widely reported for
268 other aromatic pollutants [3,10].

269 **4. Conclusions**

This study has confirmed the viability of an FTO/ZnO/TiO_2/Ag_2Se thin-film photoanode to quickly and completely remove drug residues from water at natural pH. NPX was degraded in sulfate medium by visible-light PEC at E_{anod} = +1.0 V/Ag|AgCl. Comparison with EO and PC trials has demonstrated that the PEC degradation entails synergistic phenomena. In all cases, the concentration decay obeyed a pseudo-first-order reaction. In PEC, the drug removal was slower as the drug concentration was increased, but in turn this enhanced the oxidation power due to the deceleration of the parasitic reactions of M($^{\bullet}$OH) and P($^{\bullet}$OH). The presence of a high Cl^- concentration accelerated the drug degradation because of the electrocatalytic ability of the photoanode to generate active chlorine. The NPX transformation to four main naphthalenic derivatives has been evidenced by LC-QToF-MS.

Acknowledgments

The authors thank financial support from project CTQ2016-78616-R (AEI/FEDER, EU). K. Changanaqui gratefully acknowledges PhD Program 237-215 (FONDECyT, Peru).

References

[1] J. Rivera-Utrilla, M. Sánchez-Polo, M.O. Ferro-García, G. Prados-Joya, R. Ocampo-Pérez, Pharmaceuticals as emerging contaminants and their removal from water. A review, Chemosphere 93 (2013) 1268-1287.

[2] Y. Luo, W. Guo, H.H. Ngo, L.D. Nghiem, F.I. Hai, J. Zhang, S. Liang, X.C. Wang, A review on the occurrence of micropollutants in the aquatic environment and their fate and removal during wastewater treatment, Sci. Total Environ. 473-474 (2014) 619-641.

[3] E. Brillas, I. Sirés, Electrochemical removal of pharmaceuticals from water streams: reactivity elucidation by mass spectrometry. TrAC Trend Anal. Chem. 70 (2015) 112-121.

[4] M. Mezzelani, S. Gorbi, F. Regoli, Pharmaceuticals in the aquatic environments: Evidence of emerged threat and future challenges for marine organisms, Mar. Environ. Res. 140 (2018) 41-60.

[5] M. Ashfaq, Y. Li, M.S.U. Rehman, M. Zubair, G. Mustafa, M.F. Nazar, C.-P. Yu, Q. Sun Q, Occurrence, spatial variation and risk assessment of pharmaceuticals and personal care products in urban wastewater, canal surface water, and their sediments: a case study of Lahore, Pakistan, Sci. Total Environ. 688 (2019) 653-663.

[6] I.Y. López-Pacheco, A. Silva-Narváez, C. Salinas-Salazar, A. Arévalo-Gallegos, L.A. Lizarazo-Holguin, D. Barceló, H.M.N. Iqbal, R. Parra-Saldívar, Anthropogenic contaminants of high concern: existence in water resources and their adverse effects. Sci. Total Environ. 690 (2019) 1068-1088.

[7] L.A. Schaider, K.M. Rodgers, R.A. Rudel, Review of organic wastewater compound concentrations and removal in onsite wastewater treatment systems, Environ. Sci. Technol. 51 (2017) 7304-7317.

[8] D. Wojcieszynska, U. Guzik, Naproxen in the environment: its occurrence, toxicity to nontarget organisms and biodegradation, Appl. Microbiol. Biotechnol. 104 (2020) 1849-1857.

[9] T. González J.R. Domínguez, P. Palo, J. Sánchez-Martín, Conductive-diamond electrochemical advanced oxidation of naproxen in aqueous solution: optimizing the process, J. Chem. Technol. Biotechnol. 86 (2011) 121-127.

[10] G. Coria, I. Sirés, E. Brillas, J.L. Nava, Influence of the anode material on the degradation of naproxen by Fenton-based electrochemical processes, Chem. Eng. J. 304 (2016) 817-825.

316 [11] C.J.M. Chin, T.-Y. Chen, M. Lee, C.F. Chang, Y.-T. Liu, Y.-T. Kuo, Effective anodic
317 oxidation of naproxen by platinum nanoparticles coated FTO glass, J. Hazard. Mater.
318 277 (2014) 110-119.
319 [12] R.H.O. Montes, A.P. Lima, R.R. Cunha, T.J. Guedes, W.T.P. dos Santos, E. Nossol,
320 E.M. Richter, R.A.A. Munoz, Size effects of multi-walled carbon nanotubes on the
321 electrochemical oxidation of propionic acid derivative drugs: Ibuprofen and naproxen,
322 J. Electroanal. Chem. 775 (2016) 342-349.
323 [13] M. Villanueva-Rodríguez, R. Bello-Mendoza, A. Hernández-Ramírez, E.J. Ruiz-Ruiz,
324 Degradation of anti-inflammatory drugs in municipal wastewater by heterogeneous
325 photocatalysis and electro-Fenton process, Environ. Technol. 40 (2018) 2436-2445.
326 [14] D. Kanakaraju, C.A. Motti, B.D. Glass, M. Oelgemüller, Solar photolysis versus TiO_2
327 mediated solar photocatalysis: a kinetic study of the degradation of naproxen and
328 diclofenac in various water matrices, Environ. Sci. Pollut. Res. 23 (2016) 17437-17448.
329 [15] C. Regmi, Y.K. Kshetri, R.P. Pandey, S.W. Lee, Visible-light-driven S and W co-doped
330 dendritic $BiVO_4$ for efficient photocatalytic degradation of naproxen and its mechanistic
331 analysis, Mol. Catal. 453 (2018) 149-160.
332 [16] Z. Amini, M.H. Givianrad, M. Saber-Tehrani, P.A. Azar, S.W. Husain, Synthesis of N-
333 doped $TiO_2/SiO_2/Fe_3O_4$ magnetic nanocomposites as a novel purple LED illumination-
334 driven photocatalyst for photocatalytic and photoelectrocatalytic degradation of
335 naproxen: optimization and different scavenger agents study, J. Environ. Sci. Health A
336 54 (2019) 1254-1267.
337 [17] X. Zhao, J. Qu, H. Liu, Z. Qiang, R. Liu, C. Hu, Photoelectrochemical degradation of
338 anti-inflammatory pharmaceuticals at Bi_2/MoO_6-boron-doped diamond hybrid electrode
339 under visible light irradiation, Appl. Catal. B: Environ. 91 (2009) 539-545.

[18] S. Lanzalaco, I. Sirés, A. Galia, M.A. Sabatino, C. Dispenza, O. Scialdone, Facile crosslinking of poly(vinylpyrrolidone) by electro-oxidation with IrO_2-based anode under potentiostatic conditions, J. Appl. Electrochem. 48 (2018) 1343-1352.

[19] J.R. Steter, E. Brillas, I. Sirés, On the selection of the anode material for the electrochemical removal of methylparaben from different aqueous media, Electrochim. Acta 222 (2016) 1464-1474.

[20] M.G. Peleyeju, O.A. Arotiba, Recent trend in visible-light photoelectrocatalytic systems for degradation of organic contaminants in water/wastewater, Environ. Sci. Water Res. Technol. 4 (2018) 1389-1411

[21] R. Oriol, I. Sirés, E. Brillas, A.R. de Andrade, A hybrid photoelectrocatalytic/photoelectro-Fenton treatment of Indigo Carmine in acidic aqueous solution using TiO_2 nanotube arrays as photoanode, J. Electroanal. Chem. 847 (2019) 113088.

[22] R.B. Domínguez-Espíndola, C. Bruguera-Casamada, S. Silva-Martínez, R.M. Araujo, E. Brillas, I, Sirés. Photoelectrocatalytic inactivation of *Pseudomonas aeruginosa* using an Ag-decorated TiO_2 photoanode, Separ. Purif. Technol. 208 (2019) 83-91.

[23] R. Hernández, I. Olvera-Rodríguez, C. Guzmán, A. Medel, L. Escobar-Alarcón, E. Brillas, I. Sirés, K. Esquivel, Microwave-assisted sol-gel synthesis of an Au-TiO_2 photoanode for the advanced oxidation of paracetamol as model pharmaceutical pollutant, Electrochem. Commun. 96 (2018) 42-46.

[24] I. Olvera-Rodríguez, R. Hernández, A. Medel, C. Guzmán, L. Escobar-Alarcón, E. Brillas, I. Sirés, K. Esquivel, TiO_2/Au/TiO_2 multilayer thin-film photoanodes synthesized by pulsed laser deposition for photoelectrochemical degradation of organic pollutants, Separ. Purif. Technol. 224 (2019) 189-198.

[25] K. Changanaqui, E. Brillas, H. Alarcón, I. Sirés, $ZnO/TiO_2/Ag_2Se$ nanostructures as photoelectrocatalysts for the degradation of oxytetracycline in water, Electrochim. Acta 331 (2020) 135194.

[26] S. Garcia-Segura, E. Brillas, Applied photoelectrocatalysis on the degradation of organic pollutants in wastewaters, J. Photochem. Photobiol, C: Photochem. Rev. 31 (2017) 1-35.

Figure captions

Fig. 1 HRTEM images of the $ZnO/TiO_2/Ag_2Se$ composite: (a) Powder scratched out from the FTO support, at 60,000×, and (b) cross-sectional view of the aligned NRs in the thin film grown on FTO, at 15,000×. (c) HAADF-STEM cross-sectional analysis of the thin-film photoanode, alongside the elemental distribution (EELS data)

Fig. 2 (a) Normalized concentration decays and (b) their pseudo-first-order kinetic analyses during the degradation of 100 mL of solutions containing 5.0 mg L^{-1} NPX and 50 mM Na_2SO_4 at pH 5.7 and 25 ºC, using the $FTO/ZnO/TiO_2/Ag_2Se$ as anode, supported photocatalyst or photoanode. Method: Electrochemical oxidation (EO) and photoelectrocatalysis (PEC) with a Pt wire as cathode, and photocatalysis (PC). In EO and PEC, E_{anod} = +1.0 V/Ag|AgCl. In PC and PEC, a 36 W blue LED lamp was utilized to irradiate the thin-film composite

Fig. 3 Influence of NPX concentration on drug concentration removal and pseudo-first-order kinetic analysis (inset panel) upon PEC treatment of 100 mL of drug solutions with 50 mM Na_2SO_4 at pH 5.7 and 25 ºC. A cell equipped with an $FTO/ZnO/TiO_2/Ag_2Se$ photoanode (E_{anod} = +1.0 V/Ag|AgCl), exposed to a 36 W blue LED lamp, and a Pt wire cathode was used.

Fig. 4 Effect of the electrolyte composition on the normalized drug concentration decay during the PEC treatment of 100 mL of 5.0 mg L^{-1} NPX solutions at pH 5.7 and 25 ºC, using the cell and conditions described in Fig. 3. The inset panel presents the kinetic analysis.

Fig. 5 Time course of by-products detected by LC-QToF-MS under PEC conditions of Fig. 2.

Fig. 6 Proposed initial degradation route for NPX upon PEC treatment in sulfate medium.

Table 1 Percentage of NPX degradation and pseudo-first-order rate constant with the corresponding *R*-squared value for several treatments of 100 mL of drug solutions containing different electrolytes at pH 5.7 and 25 ºC, using the FTO/ZnO/TiO_2/Ag_2Se photoanode exposed to a 36 W blue LED lamp (E_{anod} = +1.0 V/Ag|AgCl) and Pt wire cathode.

Method	[NPX] (mg L^{-1})	Electrolyte	% Degradation (time (min))	k_1 (10^{-3} min^{-1})	R^2
EO [a]	5.0	50 mM Na_2SO_4	12.0 (210)	0.586	0.980
PC [b]	5.0	50 mM Na_2SO_4	51.3 (210)	3.65	0.990
PEC [c]	2.0	50 mM Na_2SO_4	100 (180)	27.3	0.976
	3.0	50 mM Na_2SO_4	100 (180)	21.0	0.988
	4.0	50 mM Na_2SO_4	100 (210)	16.4	0.983
	5.0	50 mM Na_2SO_4	100 (210)	12.6	0.993
	5.0	25 mM Na_2SO_4 + 35 mM NaCl	96.4 (210)	10.7	0.992
	5.0	70 mM NaCl	100 (150)	16.3	0.994

[a] Electrochemical oxidation (in dark conditions)

[b] Photocatalysis (no applied anodic potential)

[c] Photoelectrocatalysis (with light irradiation and anodic potential application)

Figure(s)

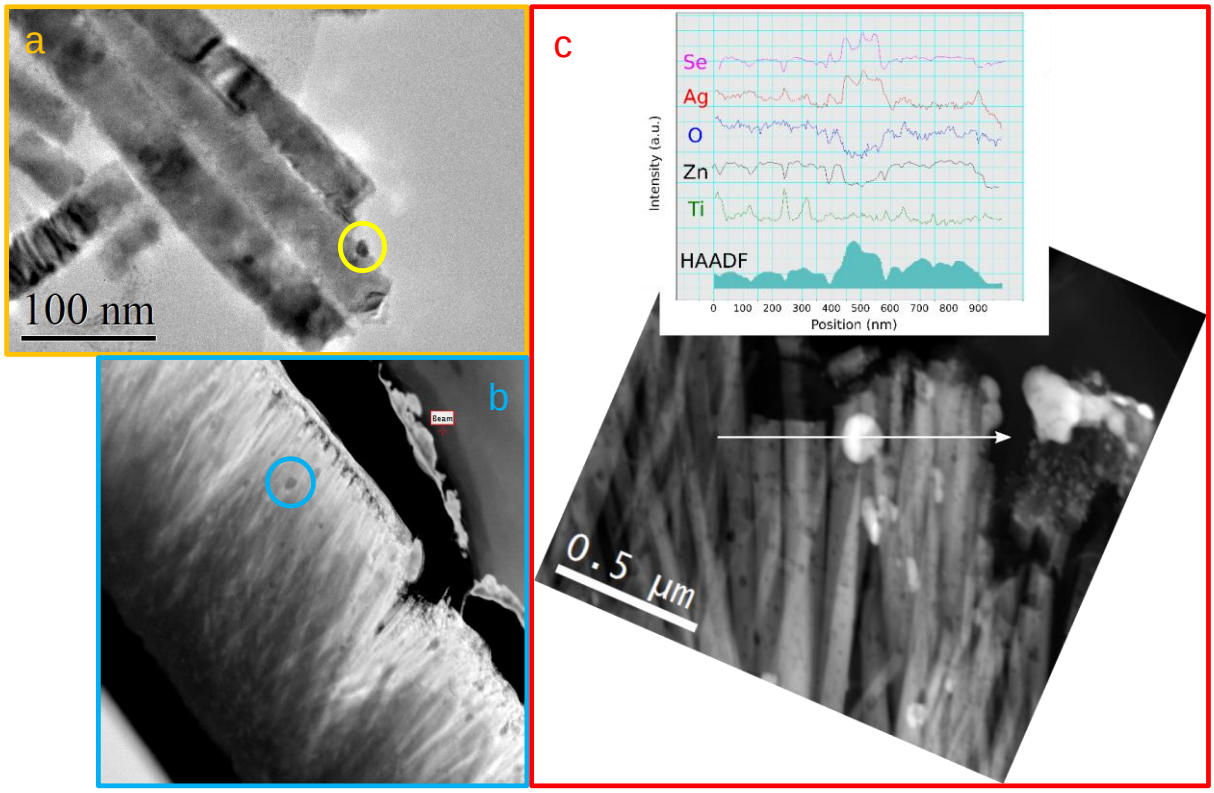

Fig. 1

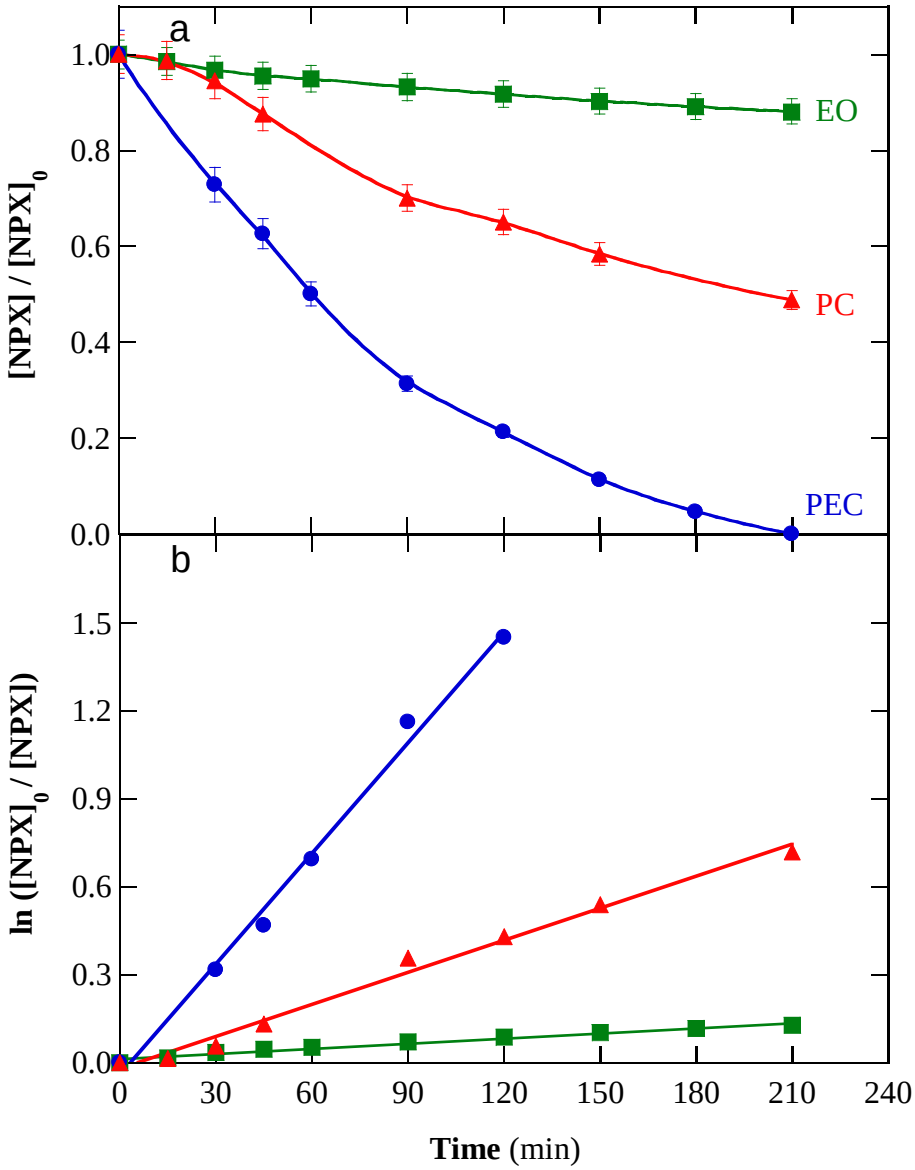
a
b
EO
PC
PEC
[NPX] / [NPX]0
ln ([NPX]0 / [NPX])
Time (min)
0.0
0.2
0.4
0.6
0.8
1.0
0.3
0.9
1.2
1.5
0
30
60
90
120
150
180
210
240

Fig. 2

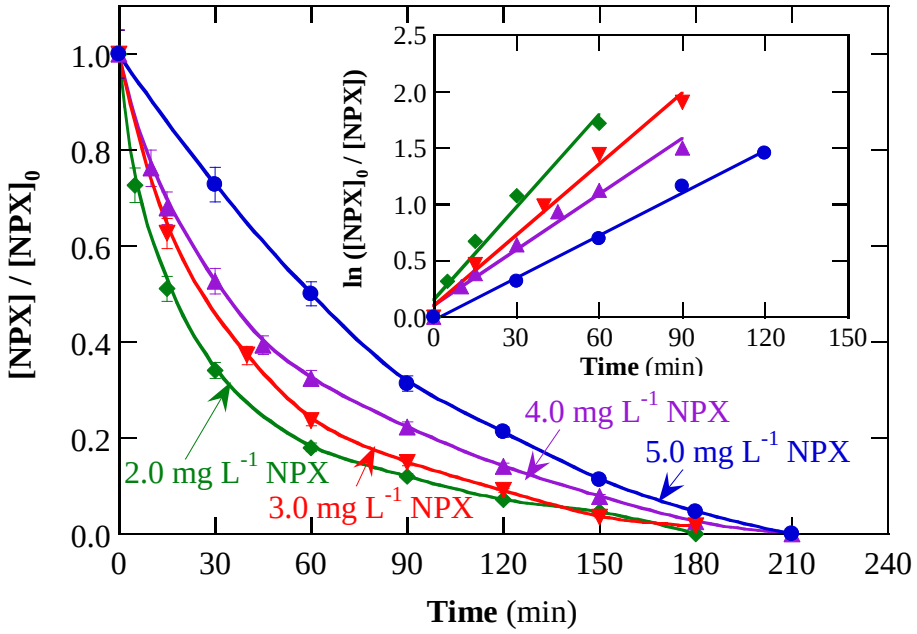
[NPX] / [NPX]0
Time (min)
ln ([NPX]0 / [NPX])
Time (min)
2.0 mg L-1 NPX
3.0 mg L-1 NPX
4.0 mg L-1 NPX
5.0 mg L-1 NPX

Fig. 3

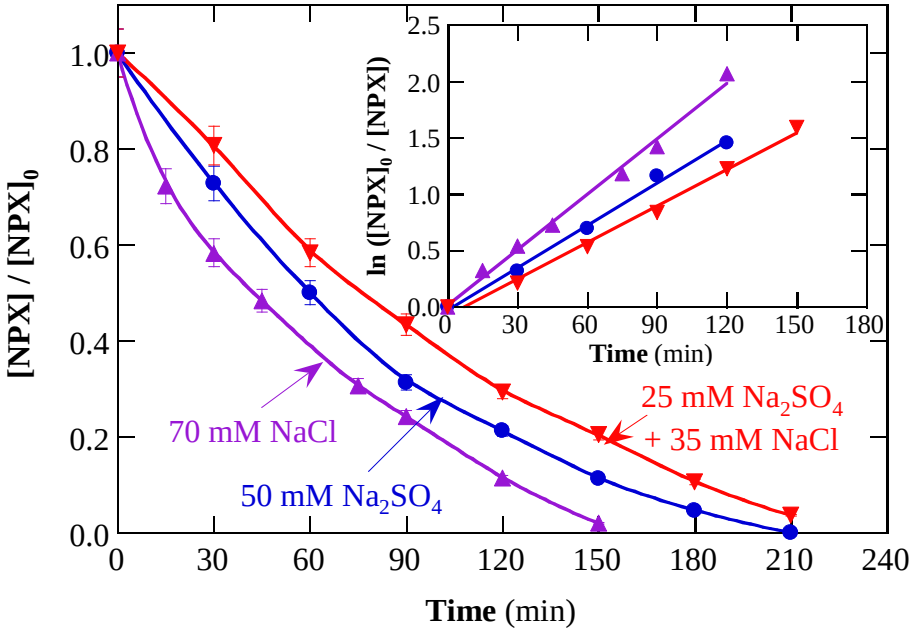
[NPX] / [NPX]0
Time (min)
70 mM NaCl
50 mM Na2SO4
25 mM Na2SO4
+ 35 mM NaCl
ln ([NPX]0 / [NPX])
Time (min)

Fig. 4

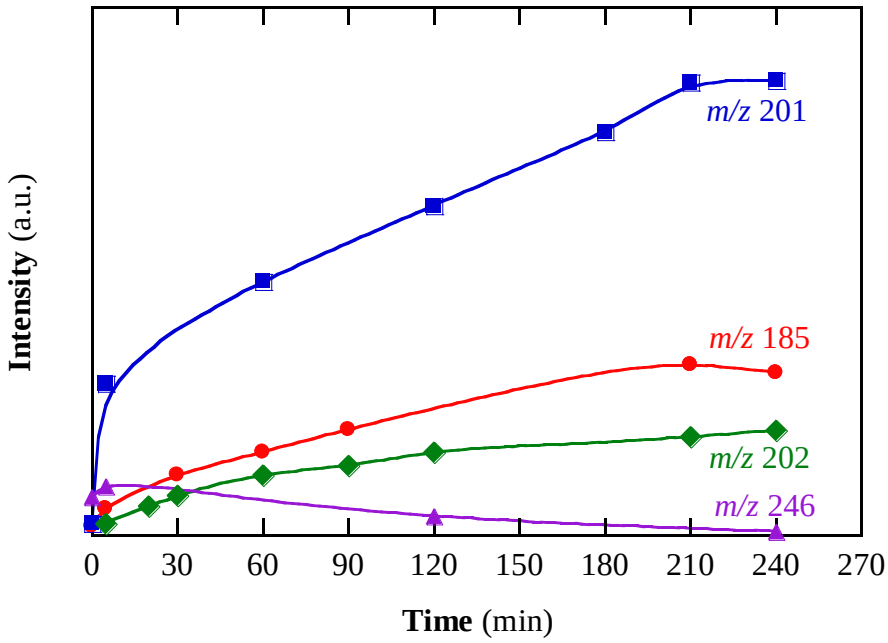
Intensity (a.u.)
m/z 201
m/z 185
m/z 202
m/z 246
0
30
60
90
120
150
180
210
240
270
Time (min)

Fig. 5

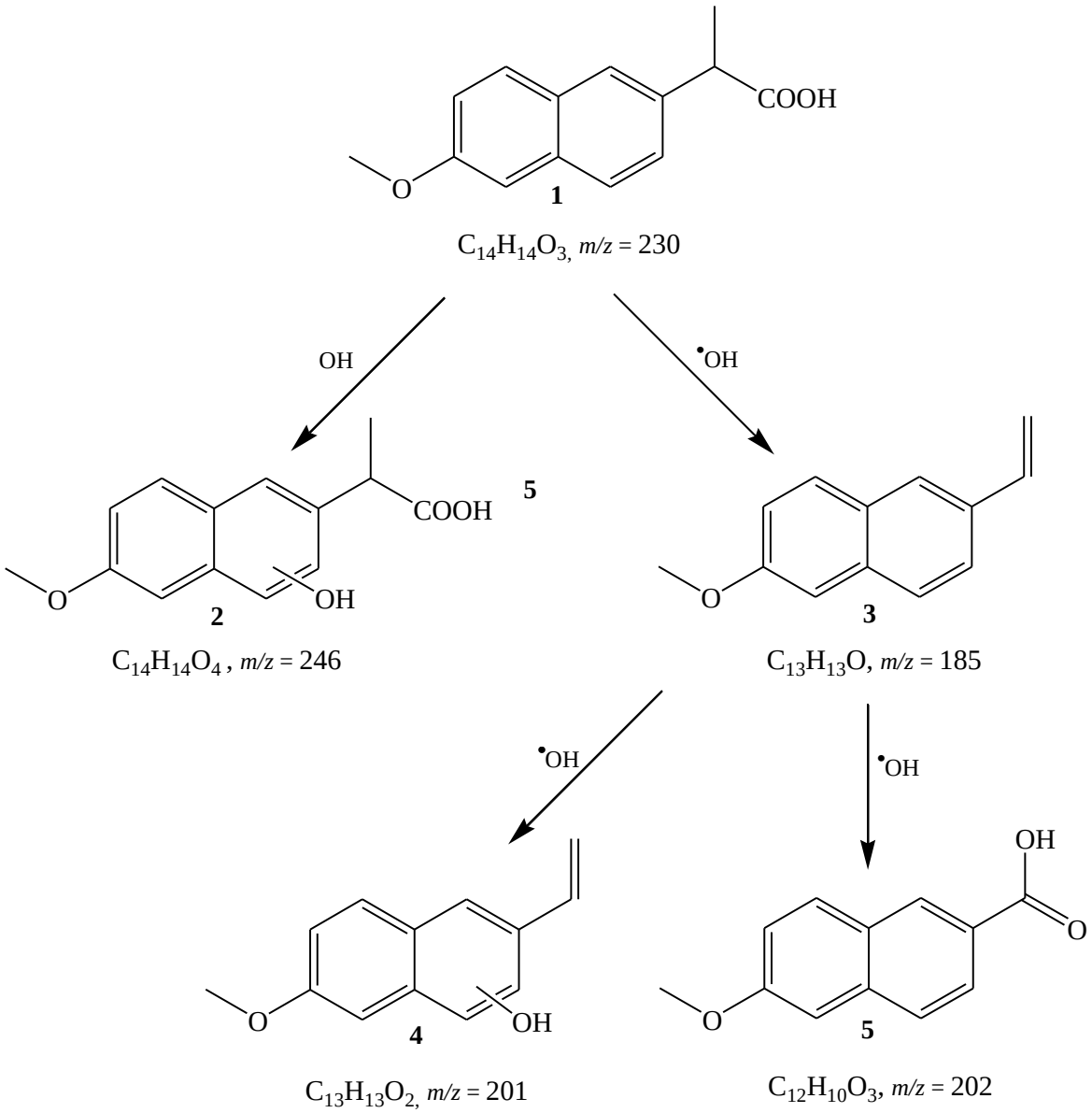
COOH
O
1
C14H14O3, m/z = 230
OH
•OH
5
COOH
O
OH
2
C14H14O4 , m/z = 246
O
3
C13H13O, m/z = 185
•OH
•OH
O
4
OH
C13H13O2, m/z = 201
OH
O
O
5
C12H10O3, m/z = 202

Fig. 6

CRediT author statement

Katherina Changanaqui: Conceptualization, Formal analysis, Investigation, Methodology; Validation; **Hugo Alarcón:** Funding acquisition; Project administration; **Enric Brillas**: Data curation, Writing; **Ignasi Sirés:** Conceptualization, Data curation, Funding acquisition; Project administration; Resources; Supervision, Writing.

***Declaration of Interest Statement**

Declaration of interests

☒ The authors declare that they have no known competing financial interests or personal relationships that could have appeared to influence the work reported in this paper.

☐The authors declare the following financial interests/personal relationships which may be considered as potential competing interests: